Original

Becherer, J.; Burchard, H.; Floeser, G.; Mohrholz, V.; Umlauf, L.:

Evidence of tidal straining in well-mixed channel flow from micro-structure observations

In: Geophysical Research Letters (2011) AGU

DOI: 10.1029/2011GL049005

Evidence of tidal straining in well-mixed channel flow from micro-structure observations

J. Becherer,[1] H. Burchard,[1] G. Flöser,[2] V. Mohrholz,[1] and L. Umlauf[1]

Received 21 July 2011; revised 15 August 2011; accepted 16 August 2011; published 15 September 2011.

[1] This study presents, for the first time, micro-structure observations in tidally energetic, weakly stratified regimes obtained in the Wadden Sea, a tidal shallow coastal area in the South-Eastern North Sea characterised by barrier islands separated by tidal gulleys. The tidal currents are typically overlaid by a weak horizontal density gradient due to freshwater run-off from land. The observations in an energetic tidal channel clearly show the expected effects of tidal straining: destratification during flood and increased stratification during ebb. Microstructure observations are consistent with the tidal straining dynamics: during the flood relatively high values of viscous dissipation are observed whilst during ebb the values are substantially smaller. It is also shown that the tidal cycle of stratification and destratification depends on the position in the tidal channel. In parts of the channel, increased stratification occurs during full flood, a phenomenon which can only be explained by advection of stratified water masses formed outside the tidal channel. The observations presented here show the general significance of the tidal straining process for tidally energetic weakly stratified regimes. **Citation:** Becherer, J., H. Burchard, G. Flöser, V. Mohrholz, and L. Umlauf (2011), Evidence of tidal straining in well-mixed channel flow from micro-structure observations, *Geophys. Res. Lett.*, *38*, L17611, doi:10.1029/2011GL049005.

1. Introduction

[2] In coastal waters, three basic dynamic regimes have been observed in tidal flows under the influence of horizontal density gradients [*Simpson et al.*, 1990; *Verspecht et al.*, 2009]: well-mixed flow during the entire tidal cycle, alternation between stratified and well mixed stages (strain-induced periodic stratification - SIPS) and permanently stratified regimes. The major parameter governing this tidal straining dynamics is the Simpson number

$$\mathrm{Si} = \frac{H^2 \partial_x b}{U_*^2}, \tag{1}$$

with the tidally averaged longitudinal buoyancy gradient, $\partial_x b$, the mean water depth, H, and a scale for the bottom friction velocity, $U_* = C_D^{1/2} U$ (with the bulk drag coefficient, $C_D \approx 2.5 \cdot 10^{-3}$ and the tidal velocity amplitude, U). In their seminal paper, *Simpson et al.* [1990] estimated threshold values for Si between these stages for Liverpool Bay based on current velocity U instead of U*. Cast into Si as defined in (1), the threshold between the well-mixed and the SIPS stages was given as $\mathrm{Si} = 8.8 \cdot 10^{-2}$ and the threshold between SIPS and permanently stratified stages was given as $\mathrm{Si} = 8.4 \cdot 10^{-1}$, i.e., of the order of unity, which means that stratifying and mixing forces are balanced [*Stacey et al.*, 2001]. The threshold values by *Simpson et al.* [1990] were shown to additionally depend on wind stress [*Verspecht et al.*, 2009] and influences of Earth rotation and relative tidal frequency [*Burchard*, 2009].

[3] The role of tidal straining on estuarine circulation and consequently on net onshore transport of suspended particulate matter (SPM) has been first described by *Jay and Musiak* [1994]. When buoyancy increases towards the coast, flood straining destabilises the water column such that mixing as well as downward momentum flux is enhanced. During ebb, mixing and downward momentum transport are reduced due to stabilisation of the water column. The tidal mean effect of this process is a near-bottom residual current directed towards the coast, strongly increasing estuarine circulation in addition to classical gravitational circulation as defined by *Hansen and Rattray* [1965] and thus significantly enhances up-estuary SPM transport [*Jay and Musiak*, 1994; *Burchard and Baumert*, 1998]. *Postma* [1954] argued that gravitational circulation, which at those times, had been discussed as the only driver of estuarine circulation does not play a significant role for net suspended matter transports in well-mixed tidal inlets and suggested processes such as settling lag as SPM transport mechanisms into the Wadden Sea, a tidal shallow coastal area in the South-Eastern North Sea. Based on a numerical model study, *Burchard et al.* [2008] however hypothesised that tidal straining may provide a much more efficient SPM transport mechanism in such highly energetic tidal environments, resulting in the generally observed accumulation of SPM in the Wadden Sea [*Pejrup*, 1997]. *Van Beusekom and de Jonge* [2002] additionally highlighted the importance of particulate organic matter import for nutrient cycling in the Wadden Sea.

[4] There has been much emphasis in recent years to study in detail the hydrodynamics and small-scale turbulence for the SIPS phenomenon [*Rippeth et al.*, 2001]. Such observations are also available for well-mixed tidal flows [*Rippeth et al.*, 2002; *Lu and Lueck*, 1999a, 1999b], but these have not been analysed for effects of horizontal density gradients. By analysing long-term current velocity profile data at small Si numbers $< 8 \cdot 10^{-2}$ (indicating well-mixed conditions), *Flöser et al.* [2011] could show that flood velocity profiles are vertically more homogeneous than ebb

[1] Leibniz Institute for Baltic Sea Research Warnemünde, Rostock, Germany.
[2] Institute for Coastal Research, Helmholtz Centre Geesthacht, Geesthacht, Germany.

0094-8276/11/2011GL049005

profiles due to tidal straining, with the asymmetry depending on the Si number. Thus, the presence of estuarine circulation can be expected even for such well-mixed flows. Using residual flow profile decomposition for idealised model simulations of tidal flow, *Burchard et al.* [2011] concluded for well-mixed flows that tidal straining has a substantially stronger impact on estuarine circulation than gravitational circulation.

[5] The major objective of the present study is to directly confirm by means of a variety of independent field observations of current velocity, temperature, salinity, small-scale turbulence and suspended matter profiles for flows with small Si numbers the significance of the tidal straining mechanism for driving estuarine circulation as sketched by *Jay and Musiak* [1994]. The study also aims at offering tidal straining as an explanation for the phenomenon of the estuarine circulation in the Wadden Sea as observed by *Flöser et al.* [2011] and as a mechanism for driving net sediment fluxes into the Wadden Sea, as hypothesised by *Burchard et al.* [2008].

2. Field Observations

2.1. Study Site

[6] The measurements were carried out in the Lister Deep, a curved tidal channel of up to 40 m depth connecting the Sylt-Rømø Bight in the northern part of the Wadden Sea with the North Sea (Figure 1). The Lister Deep transforms into a distinct ebb tidal delta in seaward direction and branches into three channels in landward direction. The average freshwater discharge per tidal cycle of two small rivers amounts to about 10^6 m^3. During the warming period in spring, horizontal thermal buoyancy gradients emerge due to differential heating of the shallow Wadden Sea water [*Burchard et al.*, 2008] such that strongest buoyancy gradient forcing is expected during April to June.

2.2. Instrumentation and Data Analysis

[7] In order to obtain some insight into the tidal straining process, a short ship campaign was carried out in the Lister Deep during April 15–17, 2008.

[8] The current velocity was measured by a vessel-mounted Acoustic Doppler Current Profiler (1200 kHz, Workhorse Broadband ADCP, Teledyne-RD Instruments). A bin resolution of 0.25 m and a sampling frequency of 0.5 Hz was used. To reduce the noise level the data were averaged over 180 s. The current vector was rotated into the current direction at the instance of strongest flood (rotated by 11° in clockwise direction with respect to east for April 15).

[9] Furthermore, a multi-probe (Sea & Sun Technology) was utilised, equipped with sensors measuring conductivity, temperature and pressure, as well as some optical quantities as fluorescence, and optical back scatter. The latter, in combination with reference suspended particulate matter (SPM) samples, is used to calculate SPM concentrations.

[10] In addition, a free-falling MSS90 micro-structure profiler (ISW Wassermeßtechnik) was used to obtain information about several turbulent parameters. The MSS90 is equipped with precision CTD sensors (Sea & Sun), a fast-response temperature sensor (FP07), pressure-sensor, as well as two airfoil shear probes (PNS06 from ISW) to analyse micro-scale vertical shear. All sensors were sampling at 1024 Hz with 16 bit resolution, while the profiler was free-falling with a speed of 0.27–0.38 m s^{-1}.

[11] Dissipation rates were obtained by integrating vertical shear spectra, assuming local isotropy in the dissipative subrange. To quantify tidally induced turbulence the friction velocity, $u_*^b = \sqrt{\tau_b/\rho_0}$, is calculated by using the law-of-the-wall scaling over the first 1.25 m above the bottom. As a measure for the stability of the water column, the potential energy anomaly ϕ has been defined by *Simpson* [1981] as the amount of mechanical energy (per m^3) required to instantaneously homogenise the water column with a given density stratification.

2.3. Field Work

[12] On April 15 and 17 fixed station measurements were carried out at S1 and S2 (Figure 1), with S1 being a shallow station (14.8 m depth) at the southern edge and S2 a deep station (23.2 m depth) near the middle of the channel. During April 16 measurements were taken along a cross-channel transect consisting of four different stations (see Tr1–Tr4 in Figure 1). The vessel was repeating this transect from south to north five times during this day. The weather conditions were stable during the whole campaign, with north-westerly winds of approximately 5 m s^{-1} during the first two days. In the night after April 16 the wind changed to north-easterly direction with approximately 5 m s^{-1} during the last day (see Figure 2a).

[13] Observations were carried out between 7 and 9 hours per day, thus not covering an entire tidal cycle, but April 15 and 17 combine to a full cycle between low waters (LW) (see gray-shaded areas in Figure 2). The measurements at station S1 contain a complete ebb (negative along-channel velocity) period and at S2 a complete flood (positive along-channel velocity) period. Generally, high water (HW) coincides with slack after flood and low water (LW) with slack after ebb (Figure 2b). During flood, salinity increases and temperature decreases and vice versa during ebb (Figure 2c), which is a clear sign for the presence of a horizontal density gradient with onshore waters being less dense than offshore waters. The density gradient is dominated by the salinity gradient with some additional contribution from temperature. By fitting the vertically integrated temperature and salinity advection equations to observations (see *Verspecht et al.* [2009] for details), average horizontal buoyancy gradients of $\partial_x b = 1.3 \cdot 10^{-6}$ s^{-2} and $\partial_x b = 0.6 \cdot 10^{-6}$ s^{-2} result for April 15 and 17, respectively. Together with the water depths given above and the maximum bottom friction velocity values of $U_* = 0.04$ m s^{-1} and $U_* = 0.05$ m s^{-1}, respectively, (1) results in Simpson numbers of Si = 0.18 and Si = 0.13 for April 15 and 17, respectively. With respect to the estimates by *Simpson et al.* [1990] both values are in the low end of the SIPS range (see section 1), such that some dynamical effects such as tidal straining and weak periodic stratification should be expected.

3. Results

[14] Figure 3 shows profiling observations obtained on April 15 at station S1. Positive current velocities in Figure 3a indicate flood, which lasts until 9:30 h (slack after flood). As seen before in Figure 2c, salinity increases and temperature decreases during flood (see Figures 3b and 3c), and vice versa during ebb.

[15] As seen from Figure 3a, the flood velocity profiles are significantly more homogeneous than the ebb profiles.

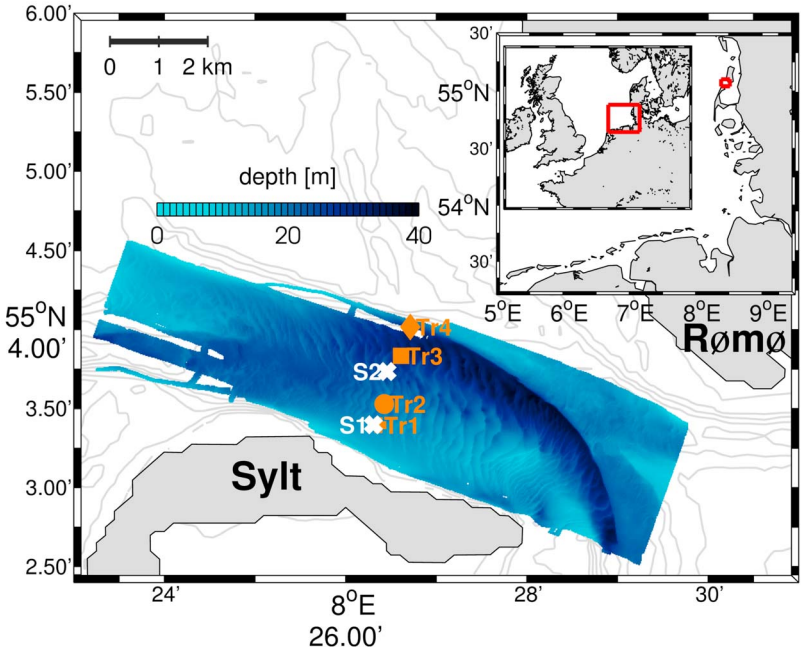

Figure 1. Map of the study-site showing water depth from multi-beam soundings (gray scale) and bathymetric charts (gray lines). S1 and S2 mark the measurement positions on April 15 and 17, respectively, and the transect stations Tr1–Tr4 (symbols) on April 16. The inserted maps show the coastlines of the North Sea (smaller map) and the German Bight areas (larger map). The transect stations are marked from south to north as cross (Tr1), circle (Tr2), square (Tr3), and diamond (Tr4).

This is quantified by the depth at which 75% of the maximum velocity of each profile are reached (note that the 50% level would be below the lowest valid ADCP observations during flood). For flood, the 75% level is −12.4 m ± 1.1 m, and for ebb this is −9.0 m ± 1.7 m. Thus, during flood, more momentum is transported downwards by means of Reynolds stress than during ebb, which directly leads to an enforcement of estuarine circulation by means of the tidal straining mechanism suggested by *Jay and Musiak* [1994]. Note that only velocity profiles after full flood and ebb, respectively, down to depth-averaged currents speeds of 0.4 m s^{-1} have been considered to only include fully developed velocity profiles. During flood (before 9:30 h) vertical stratification basically vanishes with values of $N^2 < 10^{-5}$ s^{-1} and unstable stratification in the lower half of the water column (Figure 3d). Salinity, temperature and SPM profiles are vertically almost homogeneous (Figures 3b, 3c, and 3f) due to strong vertical mixing, as indicated by high values of dissipation rate with typical values of 10^{-4} W kg^{-1} in the middle of the water column (Figure 3e). SPM concentrations show the highest concentrations during flood (≈50 mg l^{-1}), which can partially be explained by strong bottom shear stress (resulting in high resuspension rates) and high vertical mixing (resulting in vertical homogenisation). By the end of the flood (around 9:00 h), stratification increases in the upper half of the water column, in connection with decreased vertical mixing (indicated by decreased ε).

[16] At slack after flood (9:30–10:30 h), strong salinity and temperature stratification develops over the entire water column, due to exchange flow caused by horizontal buoyancy gradients, leading to peak values of $N^2 \approx 10^{-3}$ s^{-2}. The SPM concentration in the water column decreases since SPM settling is now stronger than vertical SPM mixing. For a short while, the dissipation rate is low over the entire water column ($\varepsilon < 10^{-3}$ W kg^{-1} at 9:30 h), but reaches values of $\varepsilon \approx 10^{-5}$ W kg^{-1} shortly afterwards, possibly generated by internal wave breaking.

[17] During the subsequent ebb phase, stratification remains marginally stable, with typical mid water values of $N^2 \approx 10^{-4}$ s^{-2} due to salinity and temperature stratification. Also the SPM concentration remains stratified during the entire ebb period. This is due to reduced vertical mixing

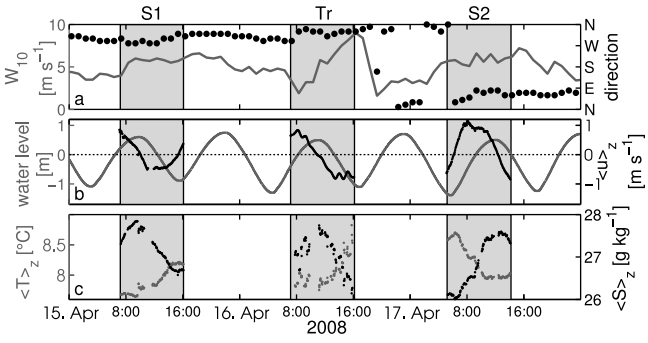

Figure 2. Observations in Lister Deep during April 15–17, 2008. (a) Wind speed (dark-gray) and direction (black dots) in List/Sylt (approximately 10 km south of the study site); (b) sea-level height (gray) in List/Sylt and depth-mean along-channel velocity component (black) from vessel-mounted ADCP; (c) vertical mean of temperature (gray) and salinity (black) from MSS and CTD. The high-lighted boxes indicate the ship-based observational periods, corresponding to the stations illustrated in Figure 1.

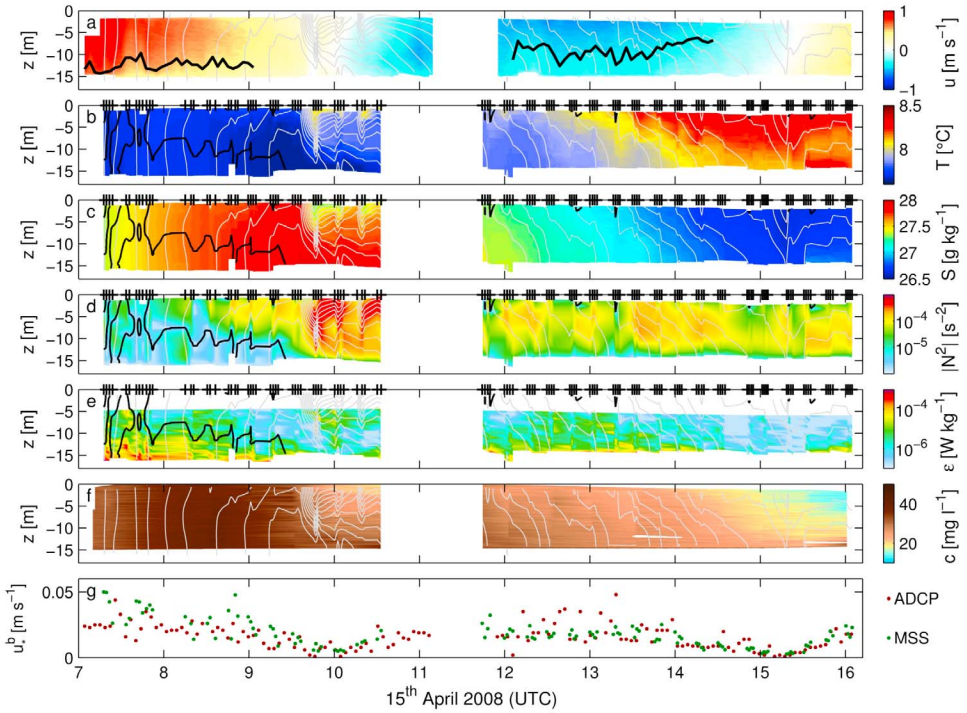

Figure 3. Observed profiles on April 15, 2008 at station S1 (see Figure 1), (a) the current velocity. (b and c) The temperature and salinity, respectively, (d) the buoyancy-frequency, N^2, and (e) the dissipation-rate of TKE. Figure 3b–3e are based on MSS-profiles, which are marked by black crosses atop the panels. (f) The SPM concentration. The bold black line in Figure 3a shows the depth level at which 75% of the velocity maximum in each profile is obtained. The light-gray lines, occurring in each panel, are isopycnals and the black line shown in Figures 3b–3e encloses areas of unstable vertical stratification ($N^2 < 0.$). (g) The temporally resolved bottom friction velocity, u_*^b, based on ADCP-data (red) and dissipation rates from the MSS (green).

since even during full ebb, around 13:00 h, the dissipation rate remains at relatively low values of $\varepsilon \approx 10^{-5}$ W kg^{-1}.

[18] During the subsequent slack tide after ebb, SPM concentrations reach a minimum, due to very low mixing ($\varepsilon \approx 10^{-7}$ W kg^{-1}). The fact that despite these low turbulence levels, stratification is not increasing during the slack after ebb (around 15:30 h), is a sign for a small value of the horizontal buoyancy gradient. This can be seen by the small decrease in density (despite prevailing ebb currents) during the last phase of ebb (14:00 h–15:00 h), see Figures 3a–3c.

[19] The temporally resolved bottom friction velocity (Figure 3g) shows good agreement between estimates from the ADCP velocity and the MSS dissipation rate, indicating maximum flood values of $u_*^b = 0.04$ m s^{-1} and somewhat smaller maximum ebb values of $u_*^b = 0.03$ m s^{-1}, with slack tides around 10:00 h and 15:30 h. Based on these data, the friction velocity scale has been estimated as $U_* = 0.04$ m s^{-1}, see section 2.3.

[20] At station S1, the potential energy anomaly ϕ shows the expected tidal cycle, with values around zero (indicating well-mixed conditions) during late flood, strong increase during slack and marginally but significantly stable values during ebb (Figure 4). Also the observations from April 16 at the two southern stations Tr1 and Tr2 along the transect show a comparable behaviour. However, the two northern transect stations Tr3 and Tr4 and also the observations at the northern anchoring station S2 taken during April 17 deviate from this classical picture. While during slack after ebb stratification increases significantly and is completely eroded during full flood (supporting the classical picture), stratification increases significantly just after full flood. On April 17, this occurs at a depth-mean flood velocity of about 0.8 m s^{-1} and at Tr3 and Tr4 on April 16 comparably high flood velocities are observed during sudden stratification (not shown). The only explanation for this atypical behaviour is lateral advection of vertically stratified water masses, probably due to topographic effects. The local effect of the change in wind direction from

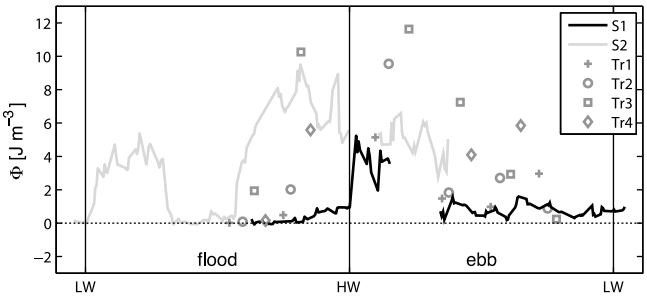

Figure 4. Potential energy anomaly, ϕ, for all profiles observed during April 15–17 in Lister Deep, with time normalised to high water (HW). The different dark gray symbols mark the certain transect stations on April 16 (see Figure 1a).

westerly to easterly after April 16 (see Figure 2a) cannot explain this phenomenon, since the surface stress at 5 m s^{-1} is very small compared to the bottom stress at 0.8 m s^{-1} current velocity.

4. Discussion and Conclusions

[21] At station S1, the dynamic impact of tidal straining is directly seen from 5 independent profiling observations: 1. velocity is mixed downwards significantly deeper during flood than during ebb; 2. temperature and 3. salinity are well mixed during flood and significantly stratified during ebb, with a maximum stratification during the slack tide in between, as indicated by N^2; 4. the SPM concentration profiles show a similar behaviour with strong homogenisation during flood and stably stratified profiles during ebb, with substantial sedimentation during slack tides; and 5. the turbulent dissipation rate is high throughout the water column during flood, but restricted to near-bottom turbulence during ebb, with decreased values during slack. The velocity data demonstrate directly the enhancement of estuarine circulation by tidal straining, supporting the quantification of this effect by numerical modelling which predicts dominance of tidal straining over gravitational circulation for low Si numbers [*Burchard et al.*, 2011]. With the data set presented here, the dynamics of tidal straining have been directly shown for the first time in a tidally energetic, weakly stratified regime. This has implications for coastal waters such as the Wadden Sea, an area for which dynamic effects of density gradients have been neglected in most of the past studies. The long term data studies by *Burchard et al.* [2008] and *Flöser et al.* [2011] have already indicated the importance of tidal straining in the Wadden Sea. There, two effects of tidal straining generate landward net SPM fluxes: the enhanced estuarine circulation and the eddy viscosity which is stronger during flood and thus moves SPM higher into the water column than during ebb. These SPM pumping mechanisms balance the seaward SPM transport caused by shear dispersion such that a landward SPM gradient is maintained.

[22] However, the observations at stations S2 (on April 17) and Tr3 and Tr4 (on April 16) with the increasing stratification just after full flood show that the dynamics may not always be as general as observed at station S1 (on April 15). It is well known that even for simple channel geometries lateral straining [see *Burchard et al.*, 2011, and references therein] can generate complex flow patterns which significantly modify along-channel straining and residual circulation. It is therefore not surprising that the classical picture is modified in the curved channel considered here in connection to its distinct ebb tidal delta in seawards direction and the branching channel system in landward direction.

[23] **Acknowledgments.** The present study has been carried out in the framework of the project ECOWS (Role of Estuarine Circulation for Transport of Suspended Particulate Matter in the Wadden Sea) funded by the German Research Foundation (DFG) as project BU1199/11. The authors are furthermore grateful for the constructive comments by Charitha Pattiaratchi and another anonymous reviewer.

[24] The Editor thanks Charitha Pattiaratchi and an anonymous reviewer for their assistance in evaluating this paper.

References

Burchard, H. (2009), Combined effects of wind, tide and horizontal density gradients on stratification in estuaries and coastal seas, *J. Phys. Oceanogr.*, *39*, 2117–2136.

Burchard, H., and H. Baumert (1998), The formation of estuarine turbidity maxima due to density effects in the salt wedge. A hydrodynamic process study, *J. Phys. Oceanogr.*, *28*, 309–321.

Burchard, H., G. Flöser, J. V. Staneva, R. Riethmüller, and T. Badewien (2008), Impact of density gradients on net sediment transport into the Wadden Sea, *J. Phys. Oceanogr.*, *38*, 566–587.

Burchard, H., R. D. Hetland, E. Schulz, and H. M. Schuttelaars (2011), Drivers of residual circulation in tidally energetic estuaries: Straight and irrotational estuaries with parabolic cross-section, *J. Phys. Oceanogr.*, *41*, 548–570.

Flöser, G., H. Burchard, and R. Riethmüller (2011), Observational evidence for estuarine circulation in the German Wadden Sea, *Cont. Shelf Res.*, in press.

Hansen, D. V., and M. Rattray (1965), Gravitational circulation in straits and estuaries, *J. Mar. Res.*, *23*, 104–122.

Jay, D. A., and J. D. Musiak (1994), Particle trapping in estuarine tidal flows, *J. Geophys. Res.*, *99*, 20,445–20,461.

Lu, Y., and R. G. Lueck (1999a), Using a Broadband ADCP in a tidal channel: Part I. Mean flow and shear, *J. Atmos. Oceanic Technol.*, *16*, 1556–1567.

Lu, Y., and R. G. Lueck (1999b), Using a Broadband ADCP in a tidal channel: Part II. Turbulence, *J. Atmos. Oceanic Technol.*, *16*, 1568–1579.

Pejrup, M. (1997), A fine-grained sediment budget for the Sylt-Rømø tidal basin, *Helgoland Mar. Res.*, *51*, 252–268.

Postma, H. (1954), Hydrography of the Dutch Wadden Sea, *Arch. Neerl. Zool.*, *10*, 405–511.

Rippeth, T. P., N. Fisher, and J. H. Simpson (2001), The semi-diurnal cycle of turbulent dissipation in the presence of tidal straining, *J. Phys. Oceanogr.*, *31*, 2458–2471.

Rippeth, T. P., E. Williams, and J. H. Simpson (2002), Reynolds stress and turbulent energy production in a tidal channel, *J. Phys. Oceanogr.*, *32*, 1242–1251.

Simpson, J. H. (1981), The shelf-sea fronts: Implications of their existence and behaviour, *Philos. Trans. R. Soc. London, Ser. A*, *302*, 531–546.

Simpson, J. H., J. Brown, J. Matthews, and G. Allen (1990), Tidal straining, density currents, and stirring in the control of estuarine stratification, *Estuaries*, *26*, 1579–1590.

Stacey, M. T., J. R. Burau, and S. G. Monismith (2001), Creation of residual flows in a partially stratified estuary, *J. Geophys. Res.*, *106*, 17,013–17,037.

van Beusekom, J. E. E., and V. N. de Jonge (2002), Long-term changes in Wadden Sea nutrient cycles: Importance of organic matter import from the North Sea, *Hydrobiologia*, *475–476*, 185–194.

Verspecht, F., T. P. Rippeth, M. J. Howarth, A. J. Souza, J. H. Simpson, and H. Burchard (2009), Processes impacting on stratification in a region of freshwater influence: Application to Liverpool Bay, *J. Geophys. Res.*, *114*, C11022, doi:10.1029/2009JC005475.

J. Becherer, H. Burchard, V. Mohrholz, and L. Umlauf, Leibniz Institute for Baltic Sea Research Warnemünde, Seestr. 15, D-18119 Rostock, Germany. (johannes.becherer@io-warnemuende.de; hans.burchard@io-warnemuende.de; volker.mohrholz@io-warnemuende.de; lars.umlauf@io-warnemuende.de)

G. Flöser, Institute for Coastal Research, Helmholtz Centre Geesthacht, Max-Planck-Str. 1, D-21502 Geesthacht, Germany. (floeser@hzg.de)